Chenguang Yin, Liancun Zheng*, Chaoli Zhang and Xinxin Zhang

Flow and Heat Transfer of Nanofluids Over a Rotating Porous Disk with Velocity Slip and Temperature Jump

Abstract: In this article, we discuss the flow and heat transfer of nanofluids over a rotating porous disk with velocity slip and temperature jump. Three types of nanoparticles – Cu, Al_2O_3 , and CuO – are considered with water as the base fluid. The nonlinear governing equations are reduced into ordinary differential equations by Von Karman transformations and solved using homotopy analysis method (HAM), which is verified in good agreement with numerical ones. The effects of involved parameters such as porous parameter, velocity slip, temperature jump, as well as the types of nanofluids on velocity and temperature fields are presented graphically and analysed.

Keywords: Homotopy Analysis; Nanofluid; Rotating Disk; Temperature Jump; Velocity Slip.

DOI 10.1515/zna-2015-0031 Received January 26, 2015; accepted March 26, 2015

1 Introduction

As one of the classical problems in fluid mechanics, the fluid flow and heat transfer over a rotating disk have been studied by many researchers in theoretical disciplines. Because of numerous practical applications in many important areas, such as computer storage devices, electronic devices, and rotating machinery, such flow is also significant in the engineering processes. Von Karman [1]

*Corresponding author: Liancun Zheng, School of Mathematics and Physics, University of Science and Technology Beijing, Beijing 100083, China, E-mail: liancunzheng@sina.com

Chenguang Yin: School of Mathematics and Physics, University of Science and Technology Beijing, Beijing 100083, China

Chaoli Zhang: School of Mathematics and Physics, University of Science and Technology Beijing, Beijing 100083, China; and School of Mechanical Engineering, University of Science and Technology Beijing, Beijing 100083, China

Xinxin Zhang: School of Mechanical Engineering, University of Science and Technology Beijing, Beijing 100083, China

firstly investigated the hydrodynamic flow over an infinite rotating disk in 1921. In his study, a famous similarity transformation was proposed to reduce the governing partial differential equations into ordinary differential equations. Cochran [2] solved the steady hydrodynamic problem formulated by Von Karman, and the asymptotic solution was established. Benton [3] considered the nonsteady flow problem on the basis of Cochran's research. Various physical features were afterwards explored [4–6]. In recent years, Shevchuk [7] studied a series of problems of convective heat and mass transfer in rotating-disk systems. Griffiths et al. [8] investigated the neutral curve for stationary disturbances in rotating disk flow for powerlaw fluids. Asghar et al. [9] considered the Lie group analysis of flow and heat transfer over a stretching rotating disk. Turkvilmazoglu [10] investigated the Bödewadt flow and heat transfer over a stretching stationary disk.

Attia [11] considered the steady flow and heat transfer over a rotating disk in porous medium, the effects of the porosity of the medium on velocity, and temperature fields. Rashidi et al. [12] presented the approximate analytical solutions by using the homotopy analysis method.

In practical applications of science and engineering, partial slip between the fluid and the moving surface may exist, for example, in the situation when the fluid is particulate such as with emulsions, suspensions, and rarefied gas. In these cases, the proper boundary condition is the partial slip. At the same time, the presence of velocity slip on the wall may cause temperature jump, which must be taken into consideration in practical applications in microscopic scale [13]. The linear slip boundary condition was first proposed by Navier [14]. Recently, Rashidi et al. [15] investigated the slip flow due to a rotating infinite disk with variable properties of the fluid. Latif [16] considered the steady laminar flow and heat transfer generated by two infinite parallel disks in the presence of velocity slip and temperature jump. Turkyilmazoglu and Senel [17] studied the traditional Von Karman swirling flow problem where the rotating disk surface admits partial slip with a uniform suction or injection.

The term "nanofluids" was introduced by Choi [18] in 1995 at the ASME Winter Annual Meeting. A nanofluid

is a colloidal mixture made by adding nanoparticles (<100 nm) in a base fluid which can considerably improve the heat transfer performance of the fluid. A list of review papers on nanofluids are given in [19–23]. Sheikholeslami [24–29] investigated a series of nanofluid flow and heat transfer problems. Bachok et al. [30] studied the steady flow of an incompressible viscous fluid over a rotating disk in a nanofluid. Rashidi et al. [31] considered the electrically conducting incompressible nanofluid flowing over a porous rotating disk with an externally applied uniform vertical magnetic field. Turkyilmazoglu [32] investigated the flow and heat transfer characteristics due to a rotating disk immersed in different nanofluids.

The homotopy analysis method (HAM) introduced by Liao in 1992 [33–38], is an effective mathematical method for solving nonlinear problems. Many studies have confirmed the effectiveness of this method. In this work, we obtain the analytical solutions by using the HAM.

The study for the flow and heat transfer of a nanofluid over a rotating porous disk, so far in our opinion, is inadequate. Especially, the partial velocity slip or temperature jump on the wall may exist, as mentioned, which must be taken into consideration in practical applications in microscopic scale. In this article we investigate the flow and heat transfer of a nanofluid over a rotating porous disk with three types of nanoparticles: Cu, CuO, and ${\rm Al_2O_3}$. The effects of porous parameter, velocity slip, temperature jump, and the types of nanofluid on velocity and temperature fields are also analysed.

2 Formulation of the Problem

We consider here an incompressible, steady, and axially symmetric nanofluid flow over a porous rotating disk. The disk is placed at $z\!=\!0$ and rotates with an angular velocity Ω through a porous medium, where the Darcy model is assumed [39]. The physical model of the rotating disk is shown in Figure 1 [30]. The governing equations of the nanofluid motion and energy in cylindrical coordinates are

$$\frac{\partial u}{\partial r} + \frac{u}{r} + \frac{\partial w}{\partial z} = 0 \tag{1}$$

$$u\frac{\partial u}{\partial r} - \frac{v^{2}}{r} + w\frac{\partial u}{\partial z} + \frac{1}{\rho_{nf}}\frac{\partial p}{\partial r} = \frac{\mu_{nf}}{\rho_{nf}}\left(\frac{\partial^{2} u}{\partial r^{2}} + \frac{1}{r}\frac{\partial u}{\partial r} - \frac{u}{r^{2}} + \frac{\partial^{2} u}{\partial z^{2}}\right)$$
$$-\frac{\mu_{nf}}{\rho_{nf}K}u$$
 (2)

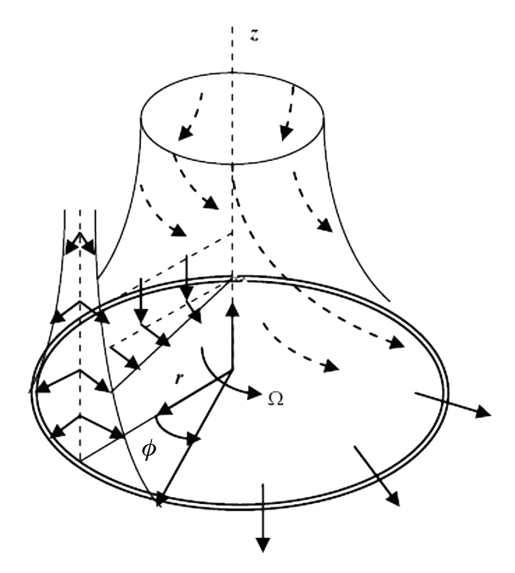


Figure 1: Physical model of rotating disk.

$$u\frac{\partial v}{\partial r} + \frac{uv}{r} + w\frac{\partial v}{\partial z} = \frac{\mu_{nf}}{\rho_{nf}} \left(\frac{\partial^2 v}{\partial r^2} + \frac{\partial}{\partial r} \left(\frac{v}{r} \right) + \frac{\partial^2 v}{\partial z^2} \right) - \frac{\mu_{nf}}{\rho_{nf} K} v \tag{3}$$

$$u\frac{\partial w}{\partial r} + w\frac{\partial w}{\partial z} + \frac{1}{\rho_{nf}}\frac{\partial p}{\partial z} = \frac{\mu_{nf}}{\rho_{nf}}\left(\frac{\partial^2 w}{\partial r^2} + \frac{1}{r}\frac{\partial w}{\partial r} + \frac{\partial^2 w}{\partial z^2}\right) - \frac{\mu_{nf}}{\rho_{nf}K}w$$
(4)

$$u\frac{\partial T}{\partial r} + w\frac{\partial T}{\partial z} = \alpha_{nf} \left(\frac{\partial^2 T}{\partial r^2} + \frac{1}{r} \frac{\partial T}{\partial r} + \frac{\partial^2 T}{\partial z^2} \right)$$
 (5)

The slip boundary conditions are given by

$$z = 0: u = \frac{2 - \sigma_u}{\sigma_u} \lambda_0 \frac{\partial u}{\partial z}, \quad v = \Omega r + \frac{2 - \sigma_u}{\sigma_u} \lambda_0 \frac{\partial v}{\partial z}, \quad w = 0,$$

$$T = T_w + \frac{2 - \sigma_T}{\sigma_x} \frac{2\beta}{1 + \beta} \frac{\lambda_0}{\Pr} \frac{\partial T}{\partial z}$$
(6)

$$z \rightarrow \infty : u \rightarrow 0, v \rightarrow 0, T \rightarrow T_{\infty}, P \rightarrow P_{\infty}$$
 (7)

where σ_u is the tangential momentum accommodation coefficient, σ_T is the thermal accommodation coefficient, λ_0 is the molecular mean free path, and β is the specific heat ratio, T is the temperature of the nanofluid, and T_∞ denotes the temperature of the ambient nanofluid, K is the Darcy permeability, the pressure is P, and the pressure of the ambient nanofluid is P_∞ . Moreover, μ_{nf} and α_{nf} are the dynamic viscosity and thermal diffusivity of the nanofluid, respectively, and ρ_{nf} is the density of the nanofluid. These are defined as

$$\mu_{nf} = \frac{\mu_{f}}{(1-\varphi)^{2.5}}, \quad \alpha_{nf} = \frac{k_{nf}}{(\rho C_{p})_{nf}} \rho_{nf} = (1-\varphi)\rho_{f} + \varphi \rho_{s}$$

$$(\rho C_{p})_{nf} = (1-\varphi)(\rho C_{p})_{f} + \varphi (\rho C_{p})_{s},$$

$$\frac{k_{nf}}{k_{f}} = \frac{(k_{s} + 2k_{f}) - 2\varphi (k_{f} - k_{s})}{(k_{s} + 2k_{f}) + \varphi (k_{f} - k_{s})}$$
(8)

in which, the nanoparticle volume fraction is denoted by φ , μ_t is the viscosity of the fluid fraction, and ρ_t and ρ_s are the densities of the fluid and of the solid fractions, respectively. The heat capacitance of the nanofluid is given by $(\rho C_n)_{nP}$ and k_{nf} stands for the effective thermal conductivity of the nanofluid approximated by the model given by Oztop and Abu-Nada [40], which is restricted to spherical nanoparticles only. The thermophysical properties of water and different nanoparticles are given in Table 1 [40].

3 Nonlinear Boundary Value **Problem**

In terms of the Von Karman's transformations,

$$\begin{split} \eta = &(\Omega/v_f)^{1/2} z, \ u = \Omega r F(\eta), \ v = \Omega r G(\eta), \ w = (\Omega v_f)^{1/2} H(\eta), \\ p - & p_{\infty} = 2\mu_f \Omega p(\eta), \ \theta(\eta) = (T - T_{\infty})/(T_w - T_{\infty}). \end{split}$$

(9)

Substituting (8) in (1)–(5) and using (9), we can obtain the following ordinary differential equations:

$$H' + 2F = 0 (10)$$

$$\left(\frac{1}{(1-\varphi)^{2.5}(1-\varphi+\varphi\rho_{s}/\rho_{f})}\right)F''-HF'-F^{2}+G^{2}-MF=0$$

$$\left(\frac{1}{(1-\varphi)^{2.5}(1-\varphi+\varphi\rho_s/\rho_f)}\right)G'' - HG' - 2FG - MG = 0 \quad (12)$$

$$\frac{1}{\Pr\left(\rho c_{p}\right)_{nf}/(\rho c_{p})_{f}}\theta'' - H\theta' = 0$$
(13)

Table 1: Thermophysical properties of water and different nanoparticles [40].

Physical properties	Pure water	Cu	CuO	Al ₂ O ₃
C_p (J/kg k)	4179	385	531.8	765
$\rho^{(kg/m^3)}$	997.1	8933	6320	3970
k (W/mk)	0.613	400	76.5	40

The transformed boundary conditions become

$$F(0) = \gamma F'(0), G(0) = 1 + \gamma G'(0), H(0) = 0, \theta(0)$$

$$= 1 + \delta \theta'(0)$$

$$F(\infty) = G(\infty) = \theta(\infty) = P(\infty) = 0$$
(14)

where $M = \mu_{nf} / K\Omega \rho_{nf}$ is the porosity parameter, $\gamma = 2 - \sigma_u / \sigma_u \lambda_0 \sqrt{\Omega / v_f}$ is the velocity slip parameter, $\delta = 2 - \sigma_T / \sigma_T (2\beta / \beta + 1) \lambda_0 / \Pr \sqrt{\Omega / \nu_f}$ is the temperature jump parameter and Pr is the Prandtl number.

The skin friction coefficient C, and the Nusselt number Nu are physical quantities which are introduced as

$$C_f = \frac{\sqrt{\tau_{wr}^2 + \tau_{w\phi}^2}}{\rho_f(\Omega r)^2}, \quad \text{Nu} = \frac{rq_w}{k_f(T_w - T_\infty)},$$
 (15)

where au_{wr} and $au_{w\phi}$ are the radial and transversal shear stress at the surface of the disk, respectively, and q_{w} is the surface heat flux, which are defined as

$$\tau_{wr} = \left[\mu_{nf}(u_z + w_{\phi})\right]_{z=0}, \quad \tau_{w\phi} = \left[\mu_{nf}\left(v_z + \frac{1}{r}w_{\phi}\right)\right]_{z=0}, \quad (16)$$

$$q_w = -k_{nf}(T_z)_{z=0}.$$

Substituting (8) in (16) and using (15), we obtain

$$\operatorname{Re}^{1/2} C_f = \frac{\sqrt{F'(0)^2 + G'(0)^2}}{(1 - \varphi)^{2.5}}, \quad \operatorname{Re}^{1/2} \operatorname{Nu} = -\frac{k_{nf}}{k_f} \theta'(0).$$
 (17)

Re = $\Omega r^2/v_s$ is the local Reynolds number.

4 HAM Solution

In this section, the HAM [33–38] is used for solving the nonlinear boundary value (10)-(14). The initial approximations are selected as

$$F_{0}(\eta) = 0, G_{0}(\eta) = e^{-\eta}/(1+\gamma)$$
 (18)

$$H_{0}(\eta) = 0, \, \theta_{0}(\eta) = e^{-\eta}/(1+\delta)$$
 (19)

The auxiliary linear operators are chosen as follows, respectively

$$\ell_1[H] = H', \quad \ell_2[F] = F'' + F', \quad \ell_3[G] = G'' + G',$$

$$\ell_{\perp}[\theta] = \theta'' + \theta'$$
(20)

Satisfying the following properties

$$\ell_{1}[c_{1}] = 0, \quad \ell_{2}[c_{2}e^{-\eta} + c_{3}] = 0, \quad \ell_{3}[c_{4}e^{-\eta} + c_{5}] = 0,$$

$$\ell_{4}[c_{6}e^{-\eta} + c_{7}] = 0$$
 (21)

(33)

where c_i , i=1–7, are the arbitrary constants. The nonlinear operators are given by

$$N_{1} = \frac{\partial H(\eta;q)}{\partial \eta} + 2F(\eta;q)$$
 (22)

$$N_{2} = C_{f} \frac{\partial^{2} F(\eta; q)}{\partial \eta^{2}} - F(\eta; q)^{2} + G(\eta; q)^{2}$$
$$-H(\eta; q) \frac{\partial F(\eta; q)}{\partial \eta} - MF(\eta; q)$$
(23)

$$\begin{split} N_{_{3}} &= C_{_{f}} \frac{\partial^{2}G(\eta;q)}{\partial\eta^{^{2}}} - H(\eta;q) \frac{\partial G(\eta;q)}{\partial\eta} - 2F(\eta;q)G(\eta;q) \\ &- MG(\eta;q) \end{split} \tag{24}$$

$$N_{4} = \frac{C_{\theta}}{\Pr} \frac{\partial^{2} \theta(\eta; q)}{\partial \eta^{2}} - H(\eta; q) \frac{\partial \theta(\eta; q)}{\partial \eta}$$
 (25)

where $q \in [0, 1]$ is the embedding parameter. The zeroorder deformation equations are constructed as the following forms

$$(1-q)\ell_{1}[H(\eta;q)-H_{0}(\eta)] = qh_{H}H_{H}(\eta)N_{1}[F(\eta;q),$$

$$G(\eta;q),H(\eta;q)]$$
(26)

$$(1-q)\ell_{2}[F(\eta;q)-F_{0}(\eta)] = qh_{F}H_{F}(\eta)N_{2}[F(\eta;q),$$

$$G(\eta;q),H(\eta;q)]$$
 (27)

$$\begin{split} &(1-q)\,\ell_{_{3}}[\,G(\eta;q)-G_{_{0}}(\eta)]=qh_{_{G}}H_{_{G}}(\eta)N_{_{3}}[\,F(\eta;q),\\ &G(\eta;q),\,H(\eta;q)] \end{split} \tag{28}$$

$$(1-q)\ell_{4}[\theta(\eta;q)-\theta_{0}(\eta)] = qh_{\theta}H_{\theta}(\eta)N_{4}[F(\eta;q),$$

$$G(\eta;q),H(\eta;q),\theta(\eta;q)]$$
(29)

with the boundary conditions

$$F(\eta;q)\Big|_{\eta=0} = \gamma \frac{\partial F(\eta;q)}{\partial \eta}\Big|_{\eta=0}, \quad G(\eta;q)\Big|_{\eta=0} = 1 + \gamma \frac{\partial G(\eta;q)}{\partial \eta}\Big|_{\eta=0}$$

$$H(\eta;q)\Big|_{\eta=0} = 0, \quad \theta(\eta;q)\Big|_{\eta=0} = 1 + \gamma \frac{\partial \theta(\eta;q)}{\partial \eta}\Big|_{\eta=0}$$
(30)

$$F(\eta;q)\Big|_{\eta=\infty} = 0, \ \theta(\eta;q)\Big|_{\eta=\infty} = 0, \ G(\eta;q)\Big|_{\eta=\infty} = 0$$
 (31)

where h_{H} , h_{r} , h_{G} , and h_{θ} denote the auxiliary nonzero parameters and $H_{H}(\eta)$, $H_{F}(\eta)$, $H_{G}(\eta)$, and $H_{\theta}(\eta)$ are the auxiliary functions.

Expanding $H(\eta;q)$, $F(\eta;q)$, $G(\eta;q)$, and $\theta(\eta;q)$ into Taylor series at q = 0, as

$$H(\eta;q) = H_0(\eta) + \sum_{m=1}^{\infty} H_m(\eta) q^m, \ F(\eta;q) = F_0(\eta)$$

$$+ \sum_{m=1}^{\infty} F_m(\eta) q^m,$$
(32)

$$G(\eta;q) = G_0(\eta) + \sum_{m=1}^{\infty} G_m \eta) q^m, \ \theta(\eta;q) = \theta_0(\eta) + \sum_{m=1}^{\infty} \theta_m(\eta) q^m,$$

where

as

$$H_{m}(\eta) = \frac{1}{m!} \frac{\partial^{m} H(\eta; q)}{\partial q^{m}} \bigg|_{q=0}, \quad F_{m}(\eta) = \frac{1}{m!} \frac{\partial^{m} F(\eta; q)}{\partial q^{m}} \bigg|_{q=0},$$
(34)

$$G_m(\eta) = \frac{1}{m!} \frac{\partial^m G(\eta;q)}{\partial q^m} \bigg|_{q=0}, \quad \theta_m(\eta) = \frac{1}{m!} \frac{\partial^m \theta(\eta;q)}{\partial q^m} \bigg|_{q=0}.$$
 (35)

Now, we derive the high-order deformation equations

$$\ell_{1}[H_{m}(\eta) - \chi_{m}H_{m-1}(\eta)] = h_{H}H_{H}(\eta)R_{1,m}(\eta)$$
(36)

$$\ell_{2}[F_{m}(\eta) - \chi_{m}F_{m-1}(\eta)] = h_{F}H_{F}(\eta)R_{2m}(\eta)$$
(37)

$$\ell_{3}[G_{m}(\eta) - \chi_{m}G_{m-1}(\eta)] = h_{G}H_{G}(\eta)R_{3,m}(\eta)$$
(38)

$$\ell_{a}[\theta_{m}(\eta) - \chi_{m}\theta_{m-1}(\eta)] = h_{a}H_{a}(\eta)R_{am}(\eta)$$
(39)

subject to the following boundary conditions

$$F_m(0) = \gamma F'_m(0), G_m(0) = \gamma G'_m(0), \theta_m(0) = \delta \theta'_m(0),$$

$$H_m(0) = 0$$
 (40)

$$F_m(\infty) = 0, G_m(\infty) = 0, \theta_m(\infty) = 0$$
 (41)

where

$$R_{1,m}(\eta) = H'_{m-1}(\eta) + 2F_{m-1}(\eta)$$
(42)

$$R_{2,m}(\eta) = C_f F_{m-1}''(\eta) - \sum_{k=0}^{m-1} F_k(\eta) F_{m-1-k}(\eta)$$

$$+ \sum_{k=0}^{m-1} G_k(\eta) G_{m-1-k}(\eta) - \sum_{k=0}^{m-1} H_k(\eta) F_{m-1-k}'(\eta) - M F_{m-1}(\eta)$$
(43)

$$R_{3,m}(\eta) = C_f G_{m-1}''(\eta) - \left[\sum_{k=0}^{m-1} H_k(\eta) G_{m-1-k}'(\eta) + 2 \sum_{k=0}^{m-1} F_k(\eta) G_{m-1-k}(\eta) \right] - M G_{m-1}(\eta)$$
(44)

$$R_{4,m}(\eta) = \frac{C_{\theta}}{\Pr} \theta_{m-1}^{"}(\eta) - \sum_{k=0}^{m-1} H_k(\eta) \theta_{m-1-k}^{'}(\eta)$$
 (45)

$$\chi_m = \begin{cases} 0 & m \le 1 \\ 1 & m \ge 2 \end{cases} \tag{46}$$

Finally, the auxiliary functions are chosen as

$$H_F(\eta) = H_G(\eta) = e^{-\eta}, H_H(\eta) = H_\theta(\eta) = 1.$$
 (47)

5 Results and Discussion

The nonlinear ordinary differential Equations (10)–(13) subjected to the boundary conditions (14) are solved analytically by HAM [33-38]. Liao [33-38] pointed out that the convergence of the HAM solutions strongly depend upon the auxiliary parameter h. By means of the h-curve, it is straightforward to choose a proper value of *h* to ensure the convergence of the solution series.

The *h*-curves of H''(0), F'(0), G'(0) and $\theta'(0)$ obtained by 10th approximation are presented in Figure 2. Moreover, the reliability of analytical results are verified with numerical ones obtained by finite difference technique [41, 42] and the results published in literatures [31] and [32], which are also shown in Table 2.

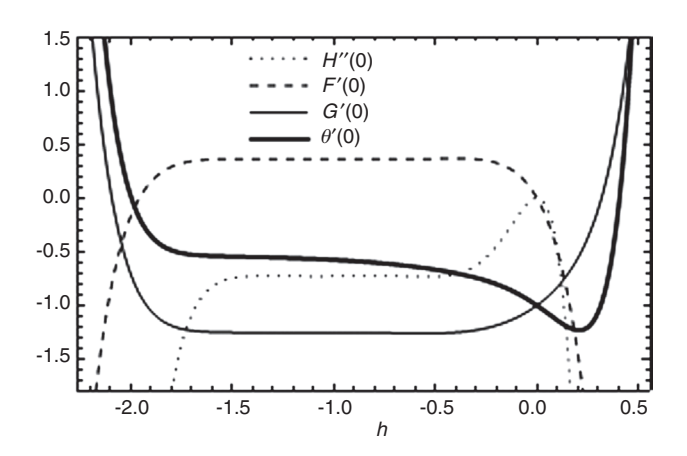


Figure 2: The *h*-curves of H''(0), F'(0), G'(0) and $\theta'(0)$ obtained by the 10th-order approximation of the HAM solution for Cu-water nanofluid, with $\varphi = 0.1$, $\gamma = 0$, $\delta = 0$, and M = 1.

Table 2: Comparison of results for F'(0), -G'(0), $-H(\infty)$ and $-\theta'(0)$, when $\varphi = 0$, M = 0, $\gamma = 0$, $\delta = 0$ and Pr = 6.2.

	Rashidi et al. [31]	Turkyilmazoglu [32]	Present
F'(0)	0.510186	0.51023262	0.51022941
-G'(0)	0.61589	0.61592201	0.61591990
-H(∞)		0.88447411	0.88446912
<i>−θ′</i> (0)		0.93387794	0.93387285

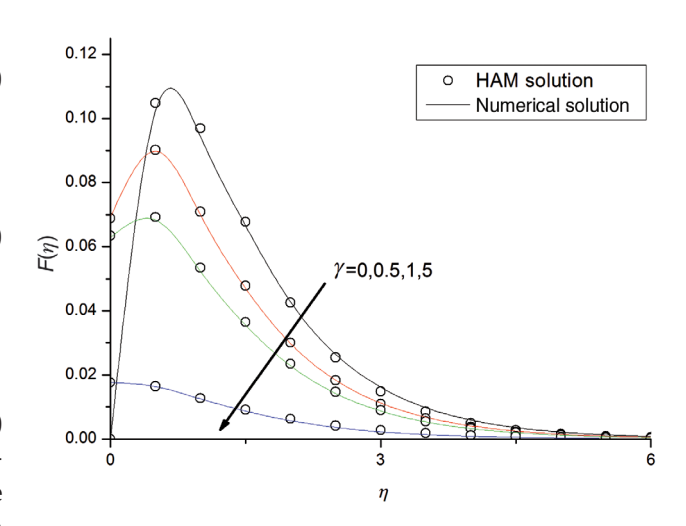


Figure 3: Effects of γ on radial velocity profiles $F(\eta)$ for Cu-water nanofluid with $\varphi = 0.1$, Pr = 6.2 and M = 0.5.

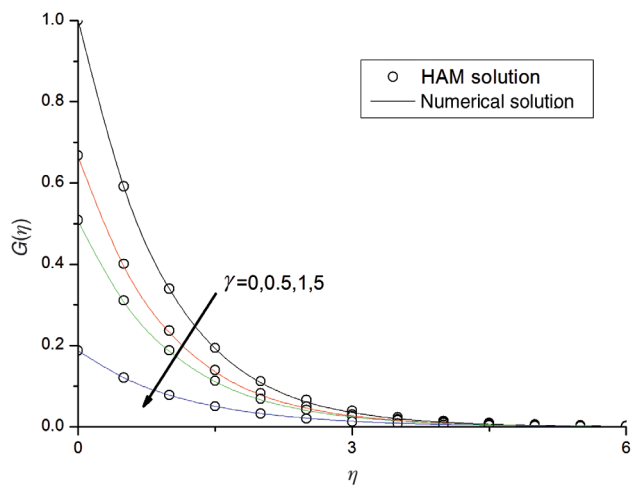


Figure 4: Effects of γ on tangential velocity profiles $G(\eta)$ for Cu-water nanofluid with $\varphi = 0.1$, Pr = 6.2 and M = 0.5.

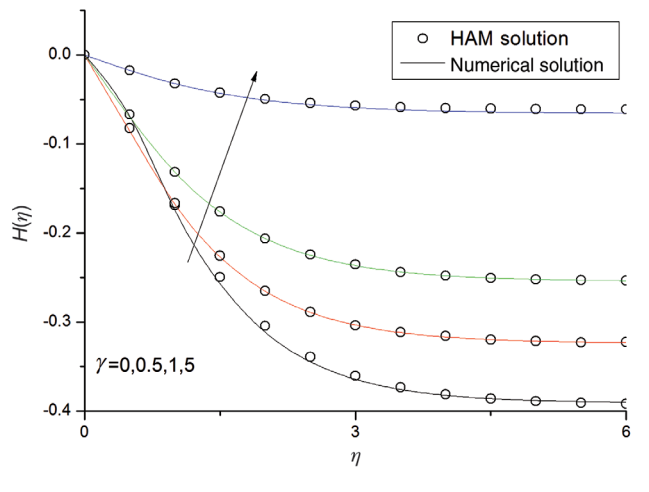


Figure 5: Effects of γ on axial velocity profiles $H(\eta)$ for Cu-water nanofluid with $\varphi = 0.1$, Pr = 6.2 and M = 0.5.

5.1 Effects of Velocity Slip Parameter

Figure 3 shows the effects of velocity slip parameter γ on the radial velocity profiles distribution. It indicates that the slip parameter has a significant effect on radial velocity distributions, there is a peak for the radial velocity profiles (maximum) which decrease rapidly and moves to the disk as the slip parameter γ increase.

Figures 4 and 5 present the variation of the tangential and axial velocity, respectively. The results indicate that, for different values of velocity slip parameter γ , the tangential velocity decreases but the axial velocity (negative) increases with the increase in γ .

In addition, Figures 3-5 present a comparison of the analytical results obtained by homotopy analysis method and the numerical solutions, the results are in a good agreement.

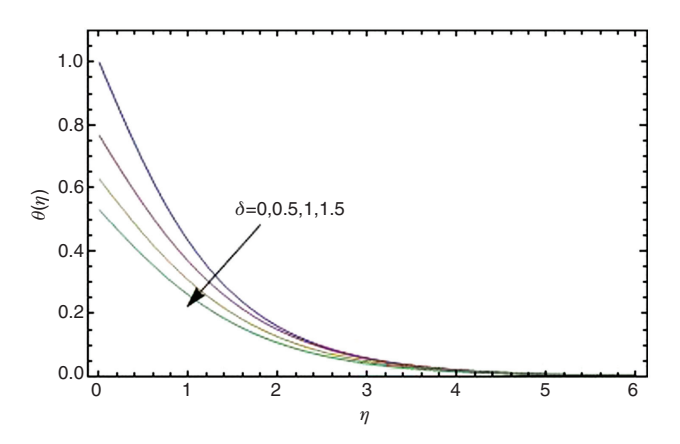


Figure 6: Effects of δ on temperature profiles $\theta(\eta)$ for Cu-water nanofluid, with $\varphi = 0.1$, Pr = 6.2 and M = 0.5.

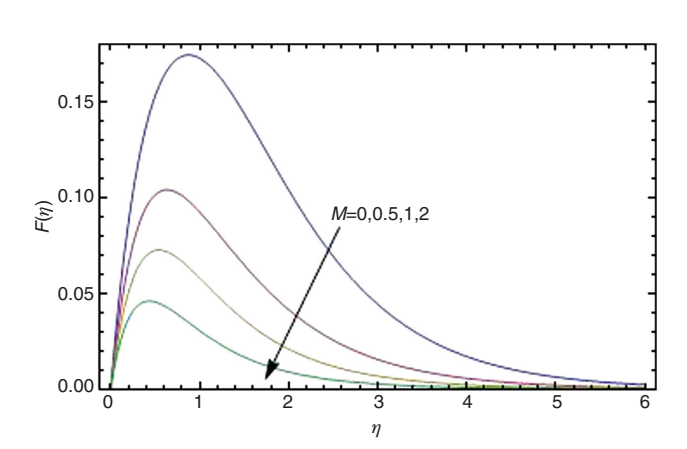


Figure 7: Effects of *M* on radial velocity profiles $F(\eta)$ for Cu-water nanofluid, with $\varphi = 0.1$, Pr = 6.2 and $\gamma = 0$.

5.2 Effects of Temperature Jump Parameter

The profiles of temperature distribution for various jump parameter δ are shown in Figure 6, the results reveal that the surface temperature and thickness of the thermal boundary layer decrease with the increasing values of δ .

The temperature jump parameter has also special effects on the local Nusselt number, it can be seen from Figure 12 that the local Nusselt number decreases with the increase in temperature jump parameter δ .

5.3 Effects of Porosity Parameter

Figures 7–10 demonstrate the effect of porosity parameter M on the velocity components in radial, tangential, and axial directions and temperature distribution. It is seen that the velocity profiles in the radial, tangential, and axial directions decrease with the increasing M, whereas the increasing M increases the thermal boundary layer thickness.

5.4 Effects of Types of Nanoparticles

The analytical results for the skin friction coefficient $Re^{1/2}C_{\epsilon}$ and the local Nusselt number Re^{-1/2} Nu, for a wide range of the nanoparticle volume fraction and three different types of nanoparticles in the presence of velocity slip and temperature jump are presented in Figures 11 and 12. It is found that the values of the skin friction coefficient and the local Nusselt number are both increase nearly linearly with the nanoparticle volume fraction. The Cu-nanofluid has the largest skin friction coefficient and heat transfer

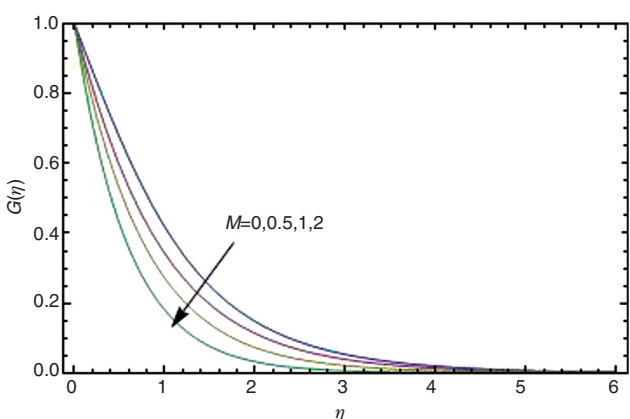


Figure 8: Effects of *M* on tangential velocity profiles $G(\eta)$ for Cu-water nanofluid, with $\varphi = 0.1$, Pr = 6.2 and $\gamma = 0$.

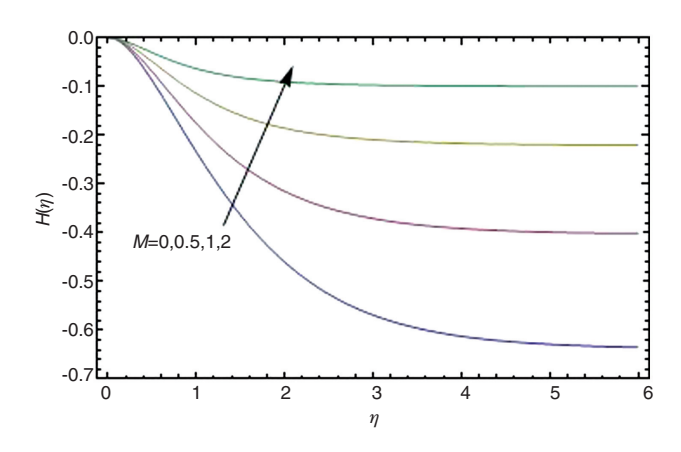


Figure 9: Effects of *M* on axial velocity profiles $H(\eta)$ for Cu-water nanofluid, with $\varphi = 0.1$, Pr = 6.2 and $\gamma = 0$.

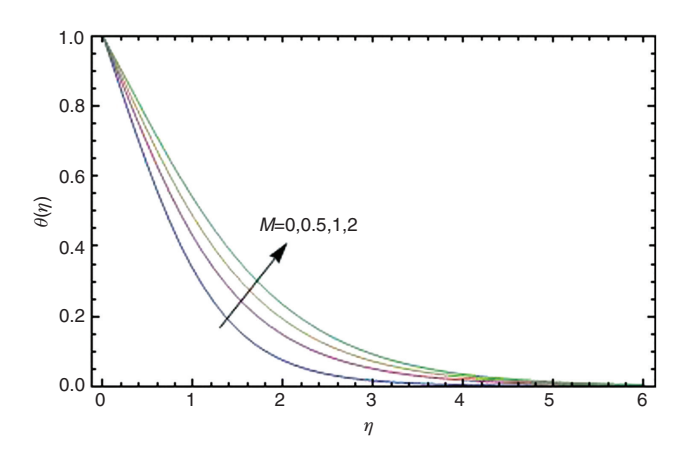


Figure 10: Effects of *M* on temperature profiles $\theta(\eta)$ for Cu-water nanofluid, with $\varphi = 0.1$, Pr = 6.2 and $\delta = 0$.

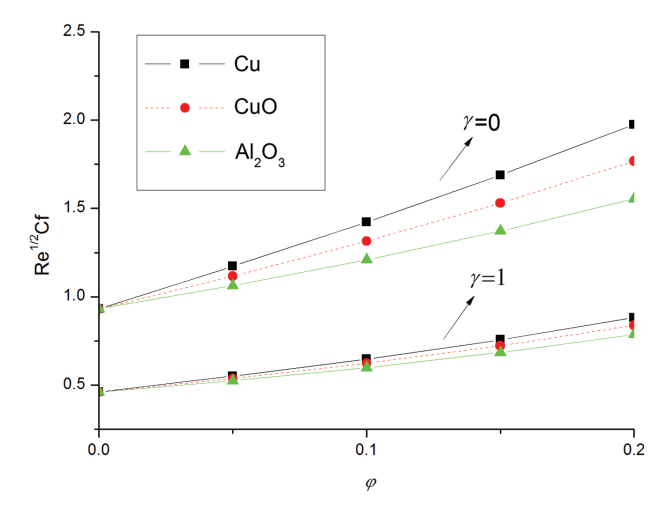


Figure 11: Variation of the skin friction coefficient with φ for different nanoparticles and velocity slip, with Pr = 6.2 and M = 0.5.

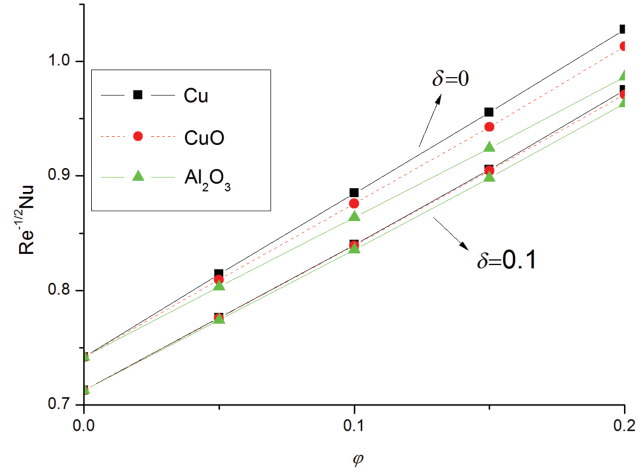


Figure 12: Variation of the Nusselt number with φ for different nanoparticles and temperature jump, with Pr = 6.2 and M = 0.5.

rate due to its largest thermal conductivity value. On the contrary, Al₂O₂-nanofluid has the lowest ones. Figure 11 indicates that the increase of velocity slip parameter γ leads to reduce the values of the skin friction coefficient. It also can be seen from Figure 12 that the local Nusselt number decreases with the increasing temperature jump parameter δ .

6 Conclusions

In this article we investigate the flow and heat transfer of nanofluid over a rotating porous disk with three types of nanoparticles: Cu, CuO, and Al₂O₃. The nonlinear governing equations are transformed into ordinary differential equations by Von Karman transformations and then solved by using the homotopy analysis method (HAM). The effects of physical parameters such as porosity parameter, velocity slip, temperature jump, and the types of nanofluid on velocity and temperature fields transport characteristics are analysed.

Acknowledgments: The work of the authors is supported by the National Natural Science Foundations of China (Numbers 51276014, 51476191).

References

- [1] T. Kármán, Z. Angew. Math. Mech. 1, 233 (1921).
- [2] W. G. Cochran, Math. Proc. Camb. Phil. Soc. 30, 365 (1934).
- [3] E. R. Benton, J. Fluid Mech. 24, 781 (1966).
- [4] H. K. Kuiken, J. Fluid Mech. 47, 789 (1971).

- [5] R. J. Lingwood, J. Fluid Mech. 299, 17 (1995).
- [6] H. A. Attia and A. L. Aboul-Hassan, Appl. Math. Model. 25, 1089 (2001).
- [7] I. V. Shevchuk, in: Lecture Notes in Applied and Computational Mechanics (Eds. F. Pfeiffer and P. Wriggers), vol. 45, Springer, 2009, p. 11.
- [8] P. T. Griffiths, S. J. Garrett, and S. O. Stephen, J. Non-Newton. Fluid Mech. 213, 73 (2014).
- [9] S. Asghar, M. Jalil, M. Hussan, and M. Turkyilmazoglu, Int. J. Heat Mass Trans. 69, 140 (2014).
- [10] M. Turkyilmazoglu, Int. J. Mech. Sci. 90, 246 (2015).
- [11] H. A. Attia, Nonlinear Anal.-Model. Contr. 14, 21 (2009).
- [12] M. M. Rashidi, S. A. Mohimanian Pour, T. Hayat, and S. Obaidat, Comput. Fluids 54, 1 (2012).
- [13] C. Hong and Y. Asako, Int. I. Heat Mass Trans. 53, 3075 (2010).
- [14] C. Navier, Mémoires de l'Académie Royale des Sciences de l'Institut de France 6, 389 (1823).
- [15] M. M. Rashidi, N. Kavyani, and S. Abelman, Int. J. Heat Mass Trans. 70, 892 (2014).
- [16] L. M. Jiji and P. Ganatos, Int. J. Heat Fluid Flow 31, 702 (2010).
- [17] M. Turkyilmazoglu and P. Senel, Int. J. Therm. Sci. 63, 146 (2013).
- [18] S. Chol, ASME-Publications-Fed 231, 99 (1995).
- [19] C. Pang, J. W. Lee, and Y. T. Kang, Int. J. Therm. Sci. 87, 49
- [20] M. Lomascolo, G. Colangelo, M. Milanese, and A. de Risi, Renew. Sust. Energ. Rev. 43, 1182 (2015).
- [21] J. Sarkar, P. Ghosh, and A. Adil, Renew. Sust. Energ. Rev. 43, 164 (2015).

- [22] R. Kamatchi and S. Venkatachalapathy, Int. J. Therm. Sci. 87, 228 (2015).
- [23] M. Bahiraei and M. Hangi, J. Magn. Magn. Mater. 374, 125 (2015).
- [24] M. S. Kandelousi, Eur. Phys. J. Plus 129, 1 (2014).
- [25] M. Sheikholeslami and D. D. Ganji, Comp. Meth. Appl. Mech. Eng. 283, 651 (2015).
- [26] M. S. Kandelousi, Phys. Lett. A378.45, 3331 (2014).
- [27] M. Sheikholeslami, J. Brazilian Soc. Mech. Sci. Eng. 1 (2014). doi: 10.1007/s40430-014-0242-z.
- [28] M. Sheikholeslami and D. D. Ganji, Energy 75, 400 (2014).
- [29] M. Sheikholeslami, M. Gorji-Bandpay, and D. D. Ganji, Int. Commun. Heat Mass Trans. 39, 978 (2012).
- [30] N. Bachok, A. Ishak, and I. Pop, Physica B: Cond. Matter 406, 1767 (2011).
- [31] M. M. Rashidi, S. Abelman, and N. Freidooni Mehr, Int. I. Heat Mass Trans. 62, 515 (2013).
- [32] M. Turkyilmazoglu, Comp. Fluids 94, 139 (2014).
- [33] S. J. Liao, Int. J. Non-Linear Mech. **30**, 371 (1995).
- [34] S. J. Liao, Eng. Anal. Bound. Elem. 20, 91 (1997).
- [35] L. Shijun, Appl. Math. Mech. 19, 957 (1998).
- [36] S. Liao, Beyond Perturbation: Introduction to the Homotopy Analysis Method, CRC Press, Boca Raton, 2003.
- [37] S. Liao, Appl. Math. Comp. 147, 499 (2004).
- [38] S. Liao, Commun. Nonlinear Sci. Num. Simu. 14, 983 (2009).
- [39] A. R. Khaled and K. Vafai, Int. J. Heat Mass Trans. 46, 4989 (2003).
- [40] H. F. Oztop and E. Abu-Nada, Int. J. Heat Fluid Flow 29, 1326
- [41] W. A. Khan and A. Aziz, Int. J. Therm. Sci. 50, 1207 (2011).
- [42] A. Aziz and W. A. Khan, Int. J. Therm. Sci. 52, 83 (2012).